Chapter 8
Three-Dimensional Particle Fields

There are two distinct challenges in the development of a multi-scale damage percolation model: (i) the development and application of the micromechanical models used to predict damage initiation and evolution and (ii) obtaining the experimental particle distributions for the model to use. While the development of the micromechanical models and implementation of the percolation model is a significant endeavour, obtaining the experimental particle distributions is equally as challenging, and arguably more tedious.

Obtaining the required experimental particle distributions remains a difficult process, especially for 3-D fields, and will often not be feasible due to cost considerations or access to the required equipment. For most materials, the basic statistics that describe the particle distribution can be reliably estimated from optical microscopy such as the average particle size, shape, spacing and volume fraction. In light of this assumption, it is of great interest to develop a particle field generator that can create representative particle fields using the experiment data (if available) or from assumed statistical distributions. The incorporation of a particle field generator into the percolation model enables fracture to be treated in a stochastic manner where the variation in the microstructure will lead to a range of predicted fracture strains.

The performance of a particle field generator rests upon knowledge of the probability density distributions for the governing variables. There are two commonly used methods to measure a particle distribution: x-ray microtomography (3-D) or from high resolution optical images (2-D). An image tessellation algorithm is then applied to extract the particle and void information such as the centroid, semi-axes, orientation and nearest neighbour information.

X-ray microtomography is the obvious choice for obtaining a three-dimensional particle distribution if the particles in the material of interest are on the order of 1 μm or larger. X-ray tomography studies of ductile fracture have long suffered from issues of resolution but recent advances have improved the resolution to about 0.7 μm at the state-of-the-art synchrotron in Grenoble, France (Maire et al. 2006; Orlov 2006). However, access to synchrotrons capable of achieving this degree of resolution is limited. As a result, obtaining 2-D images from metallographic

Z. Chen and C. Butcher, *Micromechanics Modelling of Ductile Fracture*,
Solid Mechanics and Its Applications 195, DOI 10.1007/978-94-007-6098-1_8,

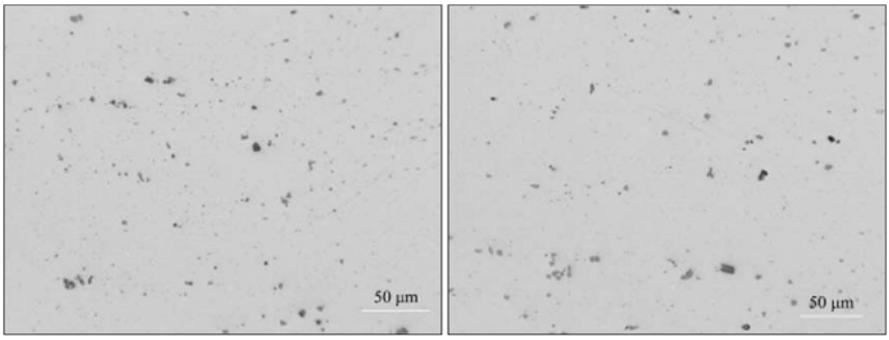

Fig. 8.1 In-plane images of the particle distribution for AA5182 sheet for a thickness of 1.0 mm (*left*) and 1.6 mm (*right*). The rolling direction is *horizontal* and the transverse direction is *vertical*

samples is the standard method of measuring a particle distribution as it is inexpensive, accessible, and has very good resolution of 0.139 µm per pixel (Chen 2004). A three-dimensional distribution can be obtained by successive sectioning of the sample and assembling the 2-D images but this is an extremely time-consuming process and may not be appropriate for materials with fine particles (Mangan et al. 1999). A typical 2-D image obtained using the sectioning and polishing method is presented in Fig. 8.1. Similarly, 3-D microtomography images are shown in Fig. 8.2 to describe the break-up of particles in AA5182 during the rolling process and in a subsequent tensile test.

This section will discuss the basic procedure for generating the particle field within the percolation model followed by sections discussing the various techniques and modeling treatments of the algorithm. Finally, the particle field generator will be used to generate representative particle fields of an aluminum-magnesium alloy and validated using the experimental results in the literature.

8.1 Particle Field Generator

The procedure for generating a particle field begins with the finite-element model. First, the algorithm identifies the elements that have been set as percolation-type elements from the input file generated using the finite-element software, LS-DYNA. The node information of these elements is used to identify the corners of the volume to determine a single element block that is termed the ‘global percolation volume’. The volume is then populated with objects based upon their packing densities and arranged into clusters. The element volume is then decomposed into its constituent elements and the individual objects are assigned to their parent element as shown in Fig. 8.3. These steps are performed automatically at the start of a finite-element simulation as part of the pre-processing routine of the percolation model. The subsequent sections will discuss the decisions and modeling treatments required in each stage of the particle generation process, starting with the sampling techniques used to define the objects.

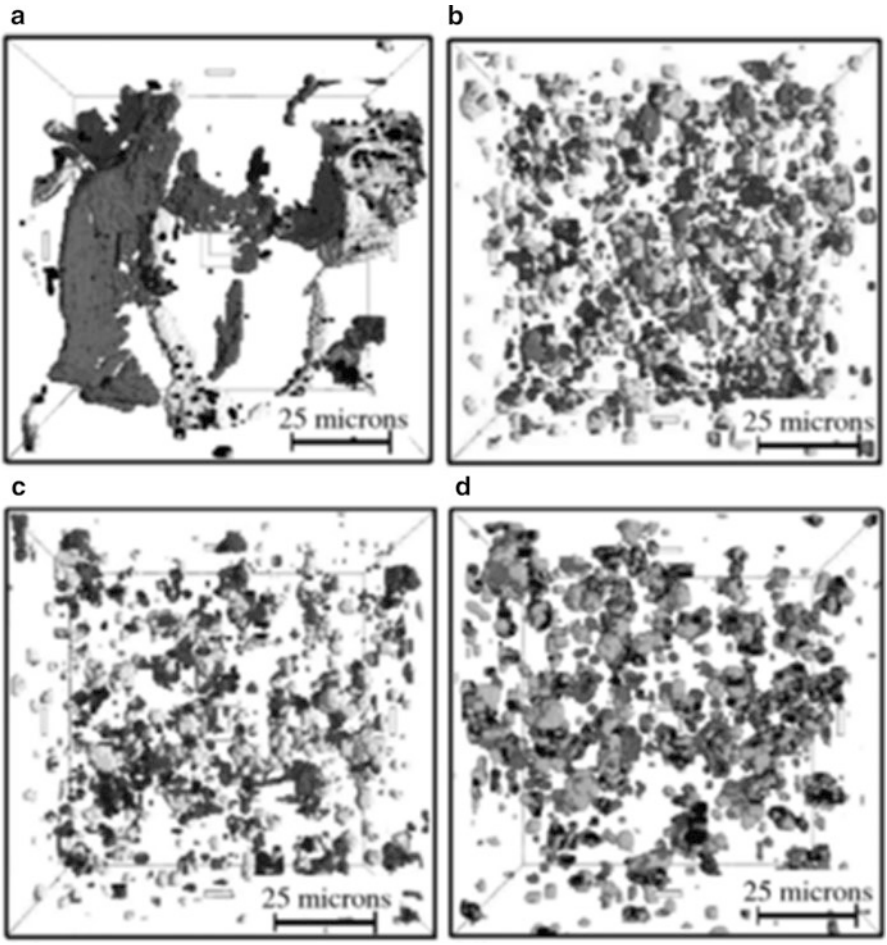

Fig. 8.2 3D view of intermetallic phases and voids in 1 mm thick AA5182 sheet obtained by Maire et al. (2006): (**a**) as cast state; (**b**) the hot rolled state; (**c**) cold rolled state; and (**d**) microstructure at the end of a tensile test. *Light grey spots* show the iron-rich particles, *dark grey spots* are Mg2Si-particles and *black spots* are pores (Reprinted with permission from Maire et al. 2006. Copyright 2006 Elsevier)

8.1.1 Particle Field Basics

Only the basics of the particle field generator developed by Butcher (2011) will be described for brevity and the interested reader is also referred to the thesis of Orlov (2006). The particle field may contain any number of particle types in addition to the voids. No restrictions are made on the properties of the particles and voids except that they must be ellipsoidal. Since the voids and particles are modeled as ellipsoids and generated using the same procedure, they will simply be referred to

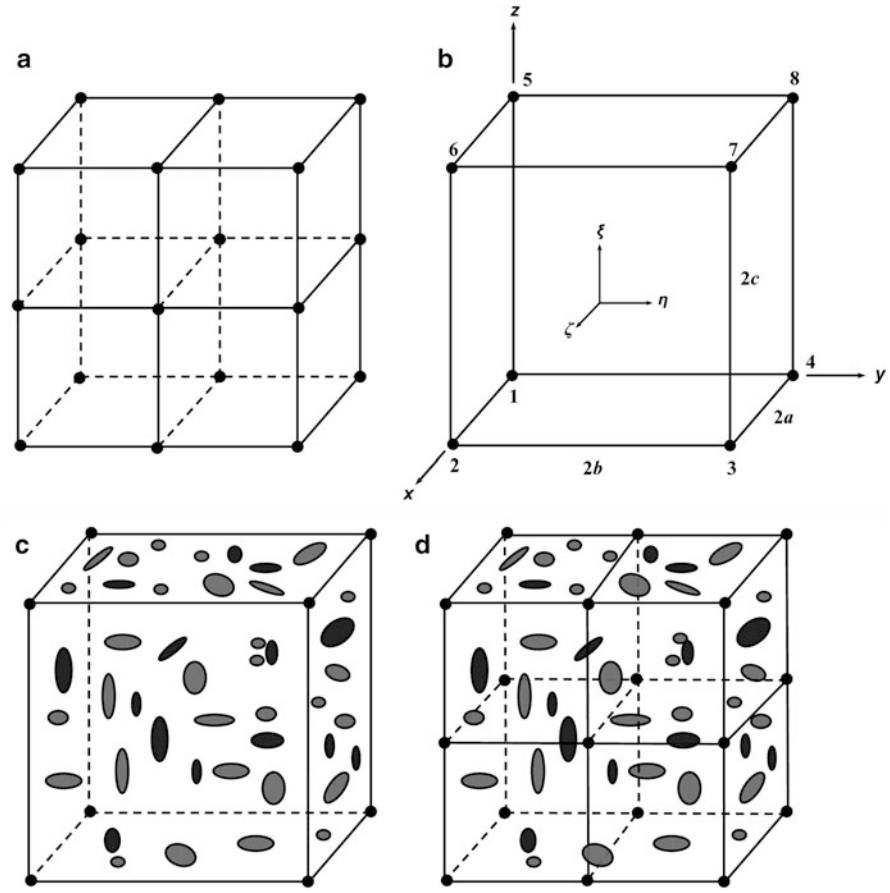

Fig. 8.3 Procedure for generating a particle field within a block of percolation elements (**a**) percolation elements identified from the global finite element mesh, (**b**) percolation elements combined to create a global element to define volume for particle field generation, (**c**) particles and voids are generated within the volume and (**d**) particles and void are assigned to parent elements

as *objects* in the proceeding sections. The procedures in this chapter are presented only for a 3-D brick element to provide a general 3-D solution but readily reduce to 2-D elements by constraining particle generation to one plane.

8.1.2 Generation of Random Variables

The particle field generator algorithm recreates the particle and void distributions through knowledge of the probability density functions (PDF) for the relevant variables such as the object semi-axes (radii), orientation angles and inter-object

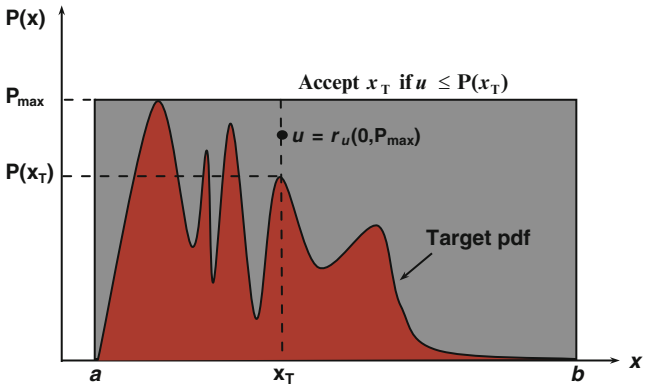

Fig. 8.4 Schematic of the rejection-sampling algorithm used to determine a random variable, x, from a target probability density function (PDF)

spacings. If the experimental distribution is known, the random variable can be generated from this distribution using a rejection-sampling technique. This method provides greater confidence in the resulting particle field since the variables of interest will have the same statistical distributions as experimentally observed. The generation of random variables from an assumed distribution such as the normal distribution is a trivial exercise and only the rejection-sampling method will be described here.

8.1.2.1 Rejection-Sampling Algorithm

A simple rejection-sampling algorithm has been adopted to obtain a random variable, x, from its experimental PDF. First, the curve data that defines the density function is pre-processed to determine maximum probability in the curve, P_{max}, as well as the left and right bounds for the variable, defined as a and b. The operation of the rejection-sampling algorithm is as follows:

- Randomly generate a trial value for the variable, x_T, that lies within $[a, b]$.
- Evaluate the probability at the trial value, $P(x_T)$, by interpolating the density curve data.
- Generate a random number, u, that lies within the range $[0, P_{max}]$.
- Accept x_T if $u \geq P(x_T)$. Otherwise, reject x_T and repeat the process with a new trial x_T.

A graphical representation of the rejection-sampling algorithm is presented in Fig. 8.4. Naturally, the resolution of the generated distribution improves with the number of samples taken. It is difficult to specify the minimum number of particles and voids to be generated in a representative volume element (RVE) because the rejection-sampling algorithm is a function of the experimental PDF. If the particle distribution exhibits multiple modes, the size of the RVE must be made larger to

increase the number of particles/voids in the element. An adaptive sampling technique may also be required for modelling complex distributions since the standard algorithm becomes computationally expensive. Conversely, well-behaved distributions can be modelled with a smaller number of samples. It is recommended that a parametric study be performed for each material of interest to establish a minimum RVE size.

8.1.3 Object Generation

8.1.3.1 Number of Objects

The number of each type of object to be generated within the volume is determined from the measured object densities, ρ_{i}, that are a measure of the number of objects per unit volume. This metric is chosen because it is easily measured experimentally compared to using volume fractions such as the porosity for the voids. This metric will lead to slight variations in the global volume fractions of the objects since the sizes of the objects will vary according to their distributions. Once the volume of the element block, V_G, has been computed, the number of objects of the i-th object type, N_{i}, to be created is

$$N_i = \rho_i(\#objects/vol)V_G \tag{8.1}$$

The use of object densities also simplifies the implementation of the algorithm because the generation process can be terminated upon reaching the desired number of objects. Alternatively, if a target volume fraction of an object is used to control the generation process, an iterative procedure would be required to continually remove and create objects to meet this target.

Generation of Object Semi-axes

All objects are general three-dimensional ellipsoids with semi-axes R_1, R_2, R_3. Since the density functions for these radii must be obtained experimentally, they correspond to a specific direction. For sheet metals, these are the rolling, transverse and short transverse or through-thickness directions. These axes could also correspond to the directions of anisotropy in a general material. The directions for the rolling, transverse and thickness directions are denoted as $\boldsymbol{r}$, $\boldsymbol{t}_{\mathrm{r}}$, and $\boldsymbol{t}_{\mathrm{t}}$, respectively. After the radii have been generated, they are sorted and reclassified into the traditional form for ellipsoids with a, b, c, as the semi-axes, where $a > b > c$.

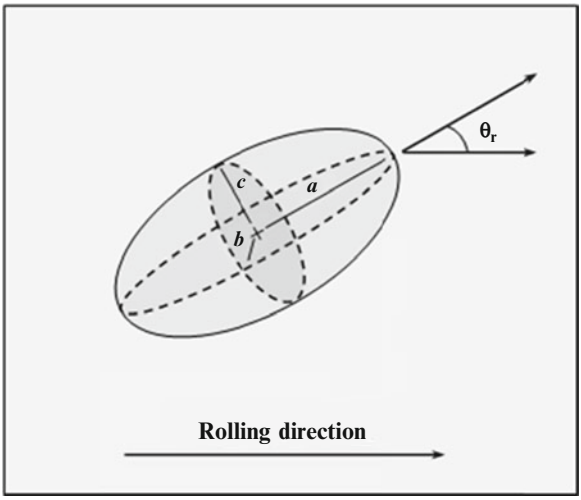

Fig. 8.5 Orientation of an object relative to the rolling direction by a solid angle, θr

Generation of Object Orientation

Unlike previous percolation models (Worswick et al. 2001; Chen 2004; Orlov 2006), no restrictions are placed upon the orientation of the objects within the field. In sheet materials, the particles and voids tend to naturally align themselves with the rolling direction. To account for the orientation of the objects, a preferential direction can be specified along with the density function for the solid angle, θ_r, from which an objects semi-major axis deviates. An example of this effect is shown in Fig. 8.5.

8.1.4 Generation of Objects Within Clusters

8.1.4.1 Object Generation Sequence

The sequence for generating the objects of a specific type can be random or follow a specific order, such as first generating all of the particles of type 1 followed by all of the particles of type 2 and then the voids. The object generation sequence plays a role in determining the degree of clustering in the material by controlling the population of available neighbours. If the object type is randomly selected, the degree of clustering of the objects will be higher as the pool of potential neighbours is kept to the current number of objects. Early in the generation process, the number of available neighbours is small and the same neighbours could be selected repeatedly, leading to excessive clustering. Conversely, if an entire population of particles is generated before a population that requires neighbours such as voids, the voids will not be as near each other as they have selected their neighbouring particle from a larger pool of potential neighbours.

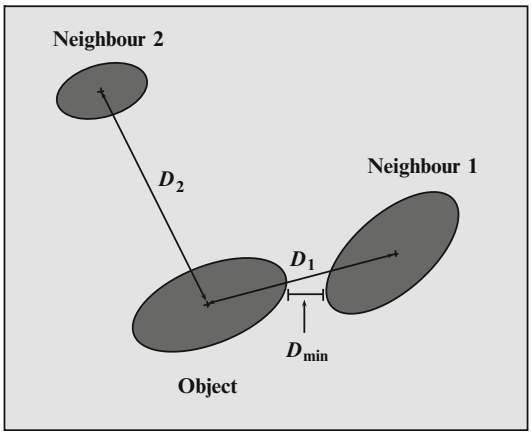

Fig. 8.6 Schematic showing the possible measures used to calculate the inter-object spacing

8.1.4.2 Distance Between Objects

Accurate knowledge of the density distributions for the distance between object types is critical to recreate the spatial distribution of the objects within the material. Experimentally, the distance between objects is commonly measured using the inter-particle dilatational spacing (IPDS) (Worswick et al. 2001; Chen 2004; Orlov 2006). This value is determined by calculating the distances between a particle or void and all of its surrounding neighbours. The minimum distance is called the IPDS and the process is repeated for all of the particles within the microstructure to develop the density function. Naturally, an IPDS distribution exists for each object and neighbour combination in the material such as IPDS distribution for voids and particles of type 1, or the distribution between particles of type 1 and type 2 and so forth. In the present work, the IPDS will be simply referred to as the inter-object spacing, denoted D_s, to provide a general term that can refer to voids or particles.

There is some uncertainty surrounding the calculation of the inter-object spacing. Typically, the spacing is taken as the minimum of all of the center-to-center distances between an object and all of its neighbours. Using this definition, $D_s = \min(D_1,D_2)$ in Fig. 8.6. However, by inspection of Fig. 8.6, it can be seen that the minimum spacing, D_{min}, between two objects can be very different compared to the center-to-center distance. The center-to-center spacing becomes a better estimate of the minimum spacing when the objects are far apart and have similar orientations.

8.1.4.3 Clusters

The voids and second-phase particles/inclusions in sheet materials are preferentially aligned in the rolling direction. Consequently, the rolling process creates aligned clusters or ‘stringers’ where neighbouring voids and particles are linearly aligned in

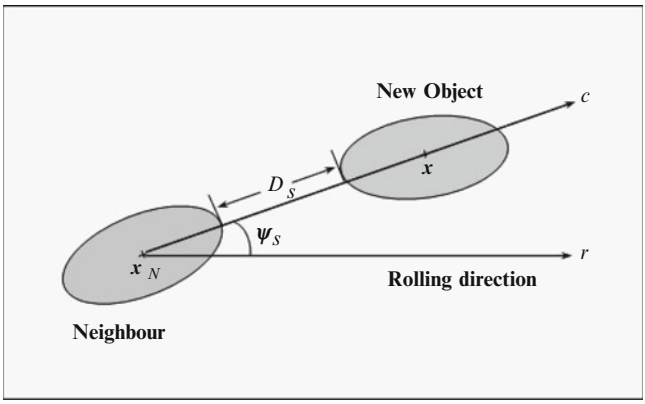

Fig. 8.7 Schematic showing the creation of a stringer-type cluster

the rolling direction. In this work, we will consider two types of clusters: general and stringer. A general cluster is formed by simply placing one object (void or particle) next to an existing object at a distance specified from the density function for the inter-object distances between the two object types. Stringer-type clusters are similar to the general type with a constraint on the location that an object can be placed next to a neighbour as shown in Fig. 8.7. An object will be placed within a general cluster when a random number from 0 to 1 is greater than the probability of clustering, P_c, such that

$$r_c(0,1) \geq \mathrm{P}_c \tag{8.2}$$

If the object has been selected to be within a cluster, then the cluster will be of the stringer-type if

$$r_s(0,1) \geq \mathrm{P}_s \tag{8.3}$$

where P_s, is the probability the object will be in a stringer-type cluster.

Object is not in a cluster: $r_c(0,1) < \mathrm{P}_c$

If the trial object does not lie within a cluster, the centroid of the object, $\boldsymbol{x}$, is randomly selected within the percolation volume.

Stringer-type cluster: $r_c(0,1) \geq \mathrm{P}_c$ and $r_s(0,1) \geq \mathrm{P}_s$

The following process is used to create a stringer-type cluster:

- An existing object is randomly selected to be the neighbour of the trial object being generated and is located at $\boldsymbol{x}_N$.
- The center-to-center vector between the two objects is denoted as $\boldsymbol{c} = (l_c, m_c, n_c)$ and the rolling direction vector is defined as $\boldsymbol{r} = (l_r, m_r, n_r)$.
- The probability density function for the stringer solid angle, ψ_s, between $\boldsymbol{c}$ and $\boldsymbol{r}$ is known for the two object types.

- The probability density function is known for the inter-object distance, D_s, between the two object types in the stringer.
- The center-to-center vector is determined that satisfies the stringer angle requirement.
- The minimum distance is computed between the ellipsoid and its neighbour. An iterative process is performed until the minimum distance along this vector is D_s. This process ensures that the two objects do not overlap and identifies the centroid, $\boldsymbol{x}$, of the object.
- If no suitable neighbour is found after a set number of attempts, a new trial object is created with a different orientation and dimensions. The neighbour search is then resumed.

General cluster: $r_c(0,1) \geq \mathrm{P}_c$ and $r_s(0,1) < \mathrm{P}_s$

If the new object is located within a general cluster, the process is the same as for the stringer cluster. The only difference between the models is in computing the center-to-center vector between the two objects. In this case, the position of the trial object, $\boldsymbol{x}$, relative to its neighbour is

$$\boldsymbol{x} = \boldsymbol{x}_N + \frac{\boldsymbol{c}(r_1(-1,1), r_2(-1,1), r_3(-1,1))}{|\boldsymbol{c}|} D_s \tag{8.4}$$

Where $\boldsymbol{c}$ is composed of three random numbers generated from a uniform distribution.

8.1.5 Particle Properties

The properties of the particles can also be assigned if their probability density functions are known. This is an important feature of the generator as the composition of the particles certainly varies in a real material and will have a significant effect on void nucleation and ultimately fracture. The distributions for the elastic modulus, E, Poisson's ratio, v, and the yield strength of the particles, σ_y, can be varied in the current version of the generator.

8.1.6 Object Constraints

An object will be rejected from the particle field if any of the following constraints are violated:

8.1.6.1 The Centroid of the Object Lies Inside the Percolation Volume

The centroid of an object, $\boldsymbol{x}$, lies within the global element block when the following constraint is true for each face:

$$\boldsymbol{n_i} \cdot \boldsymbol{x} - d_i < 0 \tag{8.5}$$

where $\boldsymbol{n}_\mathrm{i}$, are the outward facing normal vectors for the planes that define the element faces and d_i is a constant of the plane.

8.1.6.2 The Object Does Not Touch or Overlap with Any Other Object

No object is allowed to touch or overlap with another object. This constraint is enforced by evaluating the minimum distance between an object and every other object in the particle field. The objects are touching if the minimum distance is 0 or the minimum distance algorithm does not converge.

8.1.6.3 Minimum Distance Between Objects

The minimum distance between two arbitrary ellipsoids is a non-linear optimization problem that requires an iterative solution. In this work, we adopt the geometric-based algorithm of Lin and Han (2002) as it is simple, efficient and has very good convergence properties.

8.1.6.4 The Object Does Not Touch or Intersect with Any of the Facing Planes That Define the Percolation Volume

The minimum distance between an object and a plane must be determined to test if an object has intersected the boundary of the element block. This problem could be simplified to the case of testing for an intersection between a plane and ellipsoid but the minimum distance is preferred as it provides a more general solution. If the generated particle field were to be meshed in a finite-element model for homogenization studies, a minimum distance between the ellipsoids and the cell walls would have to be enforced (Pierard et al. 2007). The minimum distance between a plane and an ellipsoid can be solved by adapting the method of Lin and Han (2002). In this case, the equation of the second ellipsoid is replaced with the equation of the plane and the algorithm converges rapidly.

8.1.6.5 Neighbour Constraints

The type of permissible neighbour can be specified for each object. This information is used in modeling the clusters/nearest neighbours. The type of neighbour that an object may have is important for determining the spacing between the objects for accurate representation of object clusters. The algorithm allows for a probability distribution for the spacing between each type of neighbour in the material. This is important as the distribution for the spacing between voids and different particle types can be used in the model if they are known.

8.1.7 Identification of the Parent Element

Each object can belong to only a single parent element. An object may be intersected by the boundary between two percolation elements, but it belongs to the element in which its centroid resides. An object with its centroid at $\boldsymbol{x} = (x, y, z)$ within the global volume is located within its parent element when the following three constraints are satisfied:

$$-1 \leq \frac{x - x_c}{2a} \leq 1 \qquad -1 \leq \frac{y - y_c}{2b} \leq 1 \qquad -1 \leq \frac{z - z_c}{2c} \leq 1 \tag{8.6}$$

where x_c, y_c, z_c denote the center of the parent element that has side lengths of $2a$, $2b$, $2c$. These constraints are evaluated for each element within the element block until Eqs. (8.6a, b, c) are satisfied for the current object.

8.1.8 Numerical Implementation

The particle field generator algorithm was written in C++ and directly ported into the percolation code. A Matlab code was developed for visualization of the particle fields. The particle generator was ported into the finite-element percolation code so that a new particle field could be automatically generated at run-time. This feature provides the foundation for developing a heuristic version of the model where a large number of simulations can be performed to capture the statistical variation in the material behaviour. The algorithm for the particle field generation process is shown in Fig. 8.8.

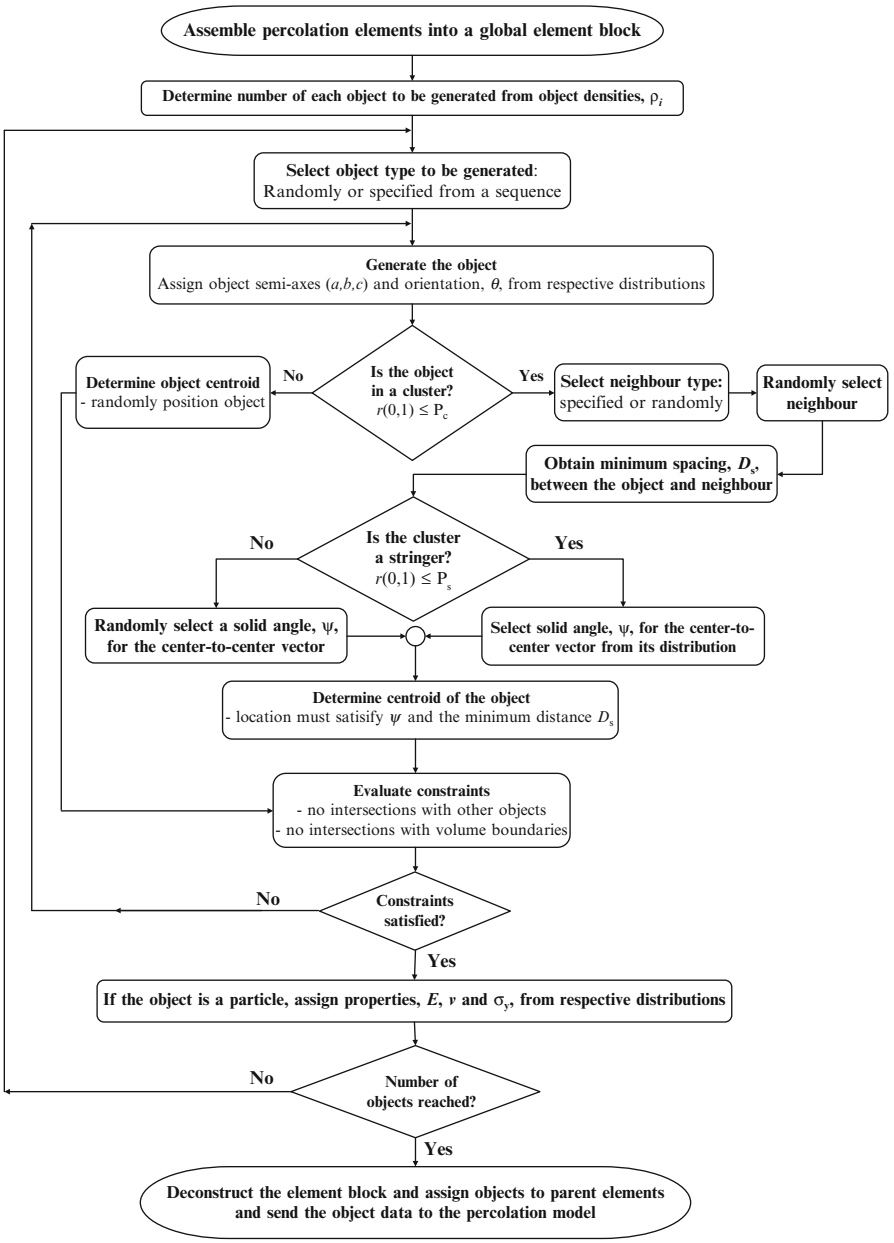

Fig. 8.8 Algorithm for the particle field generator

8.2 Application of the Particle Field Generator to an Al-Mg Alloy

Fortunately, a high-resolution x-ray microtomography study of the material of interest, AA5182 alloy, was performed by Orlov (2006). These results will be employed in the present work to generate the 3-D particle distributions for the percolation model. The resolution of the pixels within the voxel images was 0.7 μm which can capture most particles in the AA5182 sheet. Particles that are too small to be detected at this resolution are not expected to have a significant influence on the fracture strain predictions of the model because it is the large particles that will primarily nucleate voids. An experimental study of this alloy by Hadianfard et al. (2008) found that the average diameter of a broken particle (void nucleation) ranged from about 4.5 to 7.25 μm. From this study, we can conclude that the resolution used by Orlov (2006) of 0.7 μm was sufficient to capture the particles that contribute to the fracture mechanism.

8.2.1 Material Characterization

As-cast 5xxx series aluminum-magnesium alloys contain coarse intermetallic particles that may be larger than 100 μm in size. These particles then break up during the rolling process into particle fragments of 1–10 μm in size (Maire et al. 2006) as illustrated in Fig. 8.2. There are two main types of intermetallic particles in AA5182 sheet: iron-rich and Mg_2Si particles. The chemical composition of the alloy is presented in Table 8.1. The particles are oriented and elongated along the rolling direction and exhibit a strong degree of clustering. The initial voids in the material are located within particle clusters and transverse to the rolling direction, suggesting they were formed by particle cracking during the rolling process.

The tessellated particle fields were extracted from the voxel images by Orlov (2006) using a matrix erosion technique that approximated the voids and particles as ellipsoids that are aligned along the rolling, transverse or through-thickness directions of the material. The majority of the second-phase objects in AA5182 are Fe-rich (83 %), with about 10 % Mg_2Si particles located near Fe-rich particles with the remaining 7 % being voids. The object densities for the 1 mm cold rolled AA5182 sheet of Orlov (2006) are presented in Table 8.2 with the volume fractions in Table 8.3. The proximity of the voids to the particles was measured by the number of particle-void interfaces (PVI).

Overall, the percentages of the voids that shared an interface with the Fe-rich and Mg_2Si particles were reported as 46 and 54 %, respectively. This result indicates that the probability of a void nucleating during the cold rolling process is approximately equal for both particle types. This is a fortuitous result as no special measures must be taken in the particle generation process to position voids adjacent to a preferential particle type.

Table 8.1 Chemical composition of the AA5182-O alloy

Element	Si	Fe	Mg	Mn	Cu
Wt %	0.08	0.21	4.6	0.33	0.04

Table 8.2 Object densities (number per mm^3) in AA5182 sheet (Orlov 2006)

Fe-rich	Mg_2Si	Voids	Fe-rich PVI	Mg_2Si-PVI
659,127	77,045	55,889	28,103	33,439

Table 8.3 Volume fractions of the constituents in AA5182 sheet (Orlov 2006)

Fe-rich	Mg_2Si	Voids	Matrix
0.00483	0.000485	0.000529	0.994156

The sample volume was 70 × 70 × 70 μm

8.2.2 *Parameters Used in the Particle Field Generation Process for AA5182*

To generate particle fields that are in accordance with the experimental results of Orlov (2006), certain considerations must be made so that the predicted distributions are consistent with the measurement techniques used. For example, the objects must be aligned in the material directions since orientation was not considered in the image tessellation process. The following criteria and parameters were used in generating the particle fields.

- Volume of the particle field is 200 × 200 × 200 μm.
- All objects are aligned with the rolling, transverse and thickness directions. No orientation angle.
- Rejection-sampling will be used to generate the object semi-axes.
- All clusters are of the stringer type with a randomly selected solid angle of $-20°$ to $20°$ relative to the rolling direction.
- Fe-rich particles are generated first followed by the Mg_2Si particles and then the voids.
- The Fe-rich particles are randomly distributed within the volume.
- The probability of an Mg_2Si particle being in a cluster is 80 %. The spacing between an Mg_2Si particle and its neighbouring particle obeys a normal distribution with a mean of 0.7 μm and a standard deviation of 3 μm. These values were suggested by Orlov (2006).
- All voids are assumed to be within a cluster due to the assumption that the voids were created by the particle cracking during the rolling process.
- The center-to-center spacing between a void and its neighbouring particle is selected from a uniform distribution from 1 μm to 4.5 μm. These values were determined parameterically to give agreement with the experimental spacing distribution.

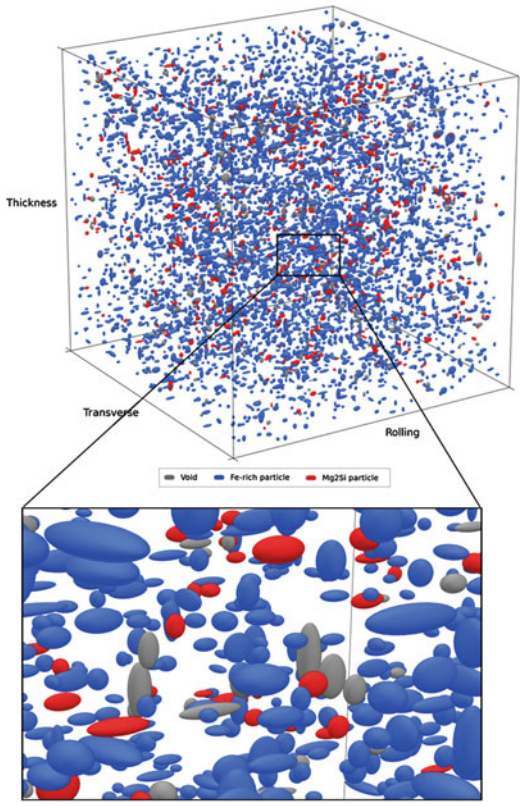

Fig. 8.9 Generated particle field of AA5182 with a volume of 200 µm × 200 µm × 200 µm

8.2.3 Particle Field Generation Results

A typical particle field with a volume of 200 × 200 × 200 µm is shown in Fig. 8.9 where the clustering of the voids and particles is evident along with their preferential orientation along the rolling direction. The number of voids, Mg_2Si and Fe-rich particles in this volume are 447, 616, 5,273, respectively. The number of objects to be created is important for the rejection-sampling algorithm to recreate the distributions for the object dimensions/properties. The resulting distribution will converge to the target distribution provided a sufficient number of random samples are taken.

8.2.4 Object Dimensions

The generated distributions for the semi-axes of the Fe-rich particles, Mg_2Si particles and voids are presented in Figs. 8.10, 8.11 and 8.12. The frequency distributions of the Fe-rich partcle dimensions are in excellent agreement with its

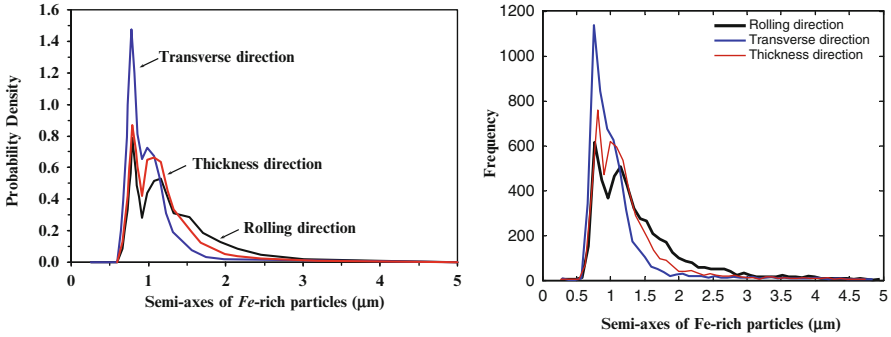

Fig. 8.10 Experimental PDF adapted from Orlov (2006) (*left*) and the generated frequency distributions for the semi-axes of the Fe-rich particles (*right*)

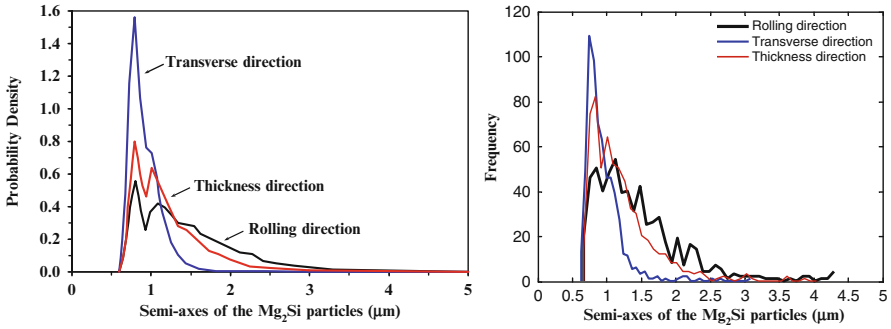

Fig. 8.11 Experimental PDF adapted from Orlov (2006) (*left*) and the generated frequency distributions for the semi-axes of the Mg2Si particles

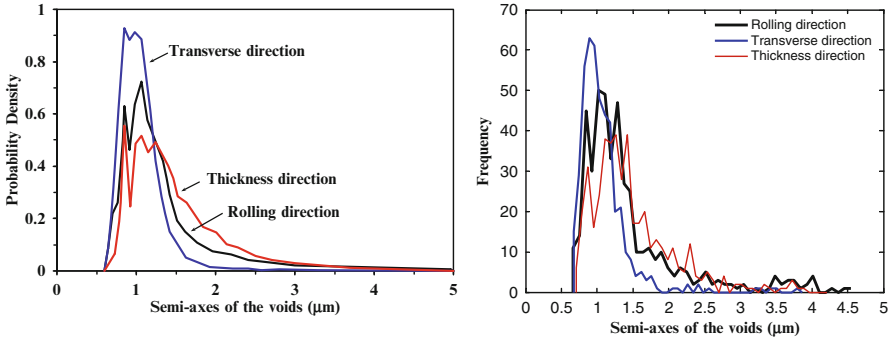

Fig. 8.12 Experimental PDF adapted from Orlov (2006) (*left*) and the generated frequency distributions for the semi-axes of the voids

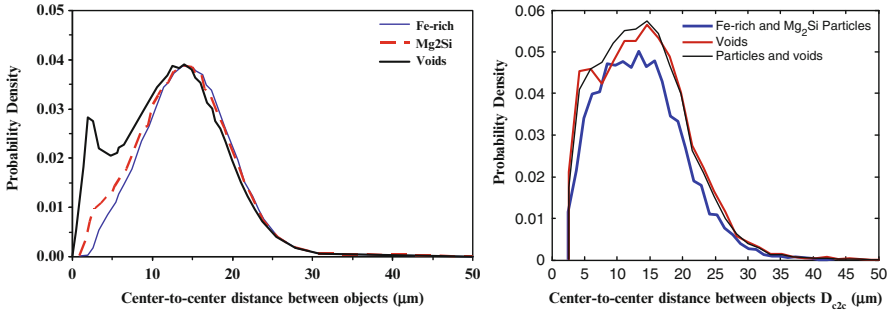

Fig. 8.13 Experimental PDF adapted from Orlov (2006) (*left*) and the generated distribution for the minimum center-to-center distance between objects

PDF distributions shown in Fig. 8.10 since 5,273 samples were taken from the target distribution in the sampling algorithm. The distributions for the Mg_2Si particles in Fig. 8.11 exhibit more scatter since only 616 particles were generated. However, the general trends are in good agreement with the experimental distribution in Fig. 8.11a and is an acceptable representation. Finally, for the voids in Fig. 6.12, the scatter is again larger compared to the Mg_2Si particles since only 447 voids are created. Nevertheless, the general trends for the void distribution can be seen when compared to the target distribution in Fig. 8.12a, especially in the transverse direction. Overall, the rejection-sampling technique employed in the present work can successfully recreate the target distribution provided a sufficient number of samples are taken. For the model alloy, decent results can be obtained with 400–600 objects and excellent agreement at 5,000 samples.

8.2.5 Spatial Distribution of the Objects

The ability of the particle field generator to recreate the spatial distribution of the objects is a true test of the performance of the algorithm since it is not a straightforward process as generating the object dimensions. The spatial distribution of the object is not explicitly controlled and is a function of the clustering parameters (probability of clustering, cluster type, allowable neighbours in the cluster), the inter-object spacing distribution functions and even the sequence that the different object populations are generated. To obtain object spacing values in accordance with the experimental results of Orlov (2006), the dimensions of the particle field must match the experimental size of 200 × 200 × 200 μm.

The probability density distributions for the spatial distributions are shown in Fig. 8.13 and are in good agreement with the experimental distributions in Fig. 5.2. A parametric study was performed to determine the inter-object spacings for the voids and their neighbouring particles since the voids exhibit a bi-modal

distribution with one strong peak at 2–4 μm and another at about 15 μm, which is the average value for all object types. A uniform distribution with a range of 1–4.5 μm enabled the distribution of the voids to exhibit the characteristic bi-modal distribution. The Fe-rich particles were generated randomly within the material and requires no assumed distribution for the particle spacing. A preliminary study for the distribution of the spacings of the Fe-particles was performed but was insensitive to the assumed values due to the large number of particles, 5,273, in the volume so that the resulting distribution for the spacings was random. For the Mg_2Si particles, a probability of clustering of 80 % with the spacing distribution following a normal distribution with a mean and standard deviation of 0.7 and 3 μm, respectively. These values were suggested by Orlov (2006). Finally, the stringer angle was varied as well but exhibited no significant influence on the resulting object-spacings. So it was assumed to vary from -20° to 20° relative to the rolling direction as this is a typical range observed in sheet metals.

Overall, the spatial distributions of the particles and voids in an AA5182 alloy can be recreated using the proposed algorithm, albiet to the accuracy of experiment data considered. It is important to mention that the clustering criterion used by Orlov (2006) is only a first-order approximation to the actual clustering in the material and could be improved in future work. The use of the minimum center-to-center object spacing provides only a rough estimate of the true clustering behaviour as it neglects the dimensions of the objects and therefore, their true spacings. The absolute minimum distance between the objects should be used in conjunction with the center-to-center distance to quantify the object spacing using a dimensionless spacing ratio. Additionally, the average spacings surrounding the objects should also be reported to obtain a radial spacing distribution. Therefore, although the particle field generator in the present work provides good agreement with the experimental distributions, the spatial reconstructions are approximate and may fail to account for certain effects.

8.2.6 Particle and Void Volume Fractions

The particle and void volume fractions are primary parameters of interest in damage-based constitutive models such as the Gurson (1977) model. While often assumed to be a material constant, it is not uncommon to see significant variation in the experimental volume fraction measurements. It is therefore of interest to generate particle fields of different sizes to observe the predicted variation of the particle and volume fractions. A total of 20 different AA5182 particle fields were generated within cubic elements with side lengths of 70, 100, 150 and 200 μm. The resulting confidence intervals for the voids and Mg_2Si particles are presented in Fig. 8.14a and the values for the Fe-rich particles in Fig. 8.14b. The general trend is that the variation in the volume fractions of the constituent objects decreases with increasing element size. As the element size increases, a larger number of objects are generated and the object dimensions consolidate about a mean value, giving rise

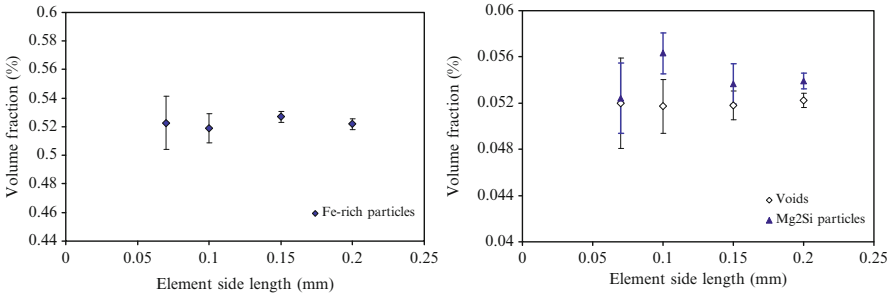

Fig. 8.14 Ninety-five percent Confidence intervals for the predicted volume fractions of the Fe-rich particles (*left*) and the voids and Mg2Si particles (*right*) in AA5182 sheet. 20 random particle fields were generated for each element volume

to a consistent prediction of the volume fraction. However, despite the decreased variation, there is no statistically significant difference because the confidence intervals overlap and we can conclude that the size of the RVE is not a significant factor when predicting the object volume fractions.

This is an interesting result since the size distributions of the objects is determined using rejection-sampling and therefore related to the element volume through the object density. This result is encouraging since the volume fraction of the voids in the element of 70 μm^3 (19 voids) is virtually the same as in the element of 200 μm^3 (447 voids). Additionally, the volume fractions for the voids, Fe-rich and Mg_2Si particles reported by Orlov (2006) for a volume of 70 μm^3 were 0.0529, 0.483 and 0.0485 %. The experimental values for the voids and Mg_2Si particles fall within the predicted range for that element size while the predictions for the Fe-rich particles are above the experimental value at about 0.525 %, which is still reasonable. The generally good agreement with the experimental volume fractions is encouraging for the performance of the particle field generator. It is also important to note that the experimental object densities were taken as constant values and future work should determine a tolerance for these values to better capture the variation in the volume fractions.

8.3 Summary

A particle field generation algorithm was developed and implemented into the percolation model to populate the elements with second-phase particles and initial voids. The particle field generator was designed for a general material and uses the probability density functions (assumed or experimental) to generate a representative particle field within the element. The particle field generator can accept any number of different particle types and accounts for the shape, orientation angle, cluster type, nearest neighbour information and particle properties.

The proposed algorithm has been implemented into the percolation model as a pre-processor to automatically create the particle distributions in the percolation elements at the start of a simulation. By generating different representative particle fields of an alloy, a series of finite-element simulations can be performed to capture the variation in the fracture strains and predicted material properties of a material of interest. The particle field generator algorithm was validated for an aluminum-magnesium alloy using the microtomography results of Orlov (2006). The void and particle size distributions, global volume fractions and inter-particle and void spacings were successfully generated by the model and in good agreement with the experimental observations.